

MESON ELASTIC AND TRANSITION FORM FACTORS

P. MARIS

*Dept. of Physics, North Carolina State University,
Box 8202, Raleigh, NC 27695-8202, USA
E-mail: pmaris@unity.ncsu.edu*

The Dyson–Schwinger equations of QCD, truncated to ladder-rainbow level, are used to calculate meson form factors in impulse approximation. The infrared strength of the ladder-rainbow kernel is described by two parameters fitted to the chiral condensate and f_π ; the ultraviolet behavior is fixed by the QCD running coupling. This obtained elastic form factors $F_\pi(Q^2)$ and $F_K(Q^2)$ agree well with the available data. We also calculate the $\rho \rightarrow \pi\gamma$ and $K^* \rightarrow K\gamma$ transition form factors, which are useful for meson-exchange models.

1. Dyson–Schwinger equations

The set of Dyson–Schwinger equations [DSEs] form a useful tool to obtain a microscopic description of hadronic properties¹. Here we use the DSEs to calculate elastic and transition form factors of the light mesons. The dressed quark propagator, as obtained from its DSE, together with the meson Bethe–Salpeter amplitude [BSA] and the dressed quark-photon vertex, form the necessary elements for calculations of form factors in impulse approximation, such as the pion elastic form factor².

The DSE for the renormalized quark propagator in Euclidean space is¹

$$S(p)^{-1} = i Z_2 \not{p} + Z_4 m(\mu) + Z_1 \int \frac{d^4 q}{(2\pi)^4} g^2 D_{\mu\nu}(p-q) \frac{\lambda^i}{2} \gamma_\mu S(q) \Gamma_\nu^i(q, p), \quad (1)$$

where $D_{\mu\nu}(k)$ is the dressed-gluon propagator and $\Gamma_\nu^i(q; p)$ the dressed-quark-gluon vertex. The most general solution of Eq. (1) has the form $S(p)^{-1} = i \not{p} A(p^2) + B(p^2)$ and is renormalized at spacelike μ^2 according to $A(\mu^2) = 1$ and $B(\mu^2) = m(\mu)$ with $m(\mu)$ the current quark mass.

Mesons are described by solutions of the Bethe–Salpeter equation [BSE]

$$\Gamma_H(p_+, p_-; Q) = \int \frac{d^4 q}{(2\pi)^4} K(p, q; Q) S(q_+) \Gamma_H(q_+, q_-; Q) S(q_-), \quad (2)$$

at discrete values of $Q^2 = -m_H^2$, where m_H is the meson mass. In this equation, $p_+ = p + \eta Q$ and $p_- = p - (1 - \eta)Q$ are the outgoing and

incoming quark momenta respectively, and similarly for q_{\pm} . The kernel K is the renormalized, amputated $q\bar{q}$ scattering kernel that is irreducible with respect to a pair of $q\bar{q}$ lines. Together with the canonical normalization condition for $q\bar{q}$ bound states, Eq. (2) completely determines the bound state BSA Γ_H . Different types of mesons, such as pseudoscalar or vector mesons, are characterized by different Dirac structures.

The quark-photon vertex, $\Gamma_{\mu}(p_+, p_-; Q)$, with Q the photon momentum and p_{\pm} the quark momenta, is the solution of the inhomogeneous BSE

$$\Gamma_{\mu}(p_+, p_-; Q) = Z_2 \gamma_{\mu} + \int \frac{d^4 q}{(2\pi)^4} K(p, q; Q) S(q_+) \Gamma_{\mu}(q_+, q_-; Q) S(q_-). \quad (3)$$

Solutions of the homogeneous version of Eq. (3) define vector meson bound states at timelike photon momenta $Q^2 = -m_V^2$. It follows that $\Gamma_{\mu}(p_+, p_-; Q)$ has poles at these locations^{2,3}.

To solve the BSE, we use a ladder truncation,

$$K(p, q; P) \rightarrow -\alpha^{\text{eff}}((p-q)^2) D_{\mu\nu}^0(p-q) \frac{\lambda^i}{2} \gamma_{\mu} \otimes \frac{\lambda^i}{2} \gamma_{\nu}, \quad (4)$$

in conjunction with the rainbow truncation for the quark DSE, Eq. (1): $\Gamma_{\nu}^i(q, p) \rightarrow \gamma_{\nu} \lambda^i / 2$ and $Z_1 g^2 D_{\mu\nu}(k) \rightarrow 4\pi \alpha^{\text{eff}}(k^2) D_{\mu\nu}^0(k)$. Here, $D_{\mu\nu}^0(k)$ is the free gluon propagator in Landau gauge, and $\alpha^{\text{eff}}(k^2)$ the effective quark-quark interaction, which reduces to the one-loop QCD running coupling $\alpha^{1\text{-loop}}(k^2)$ in the perturbative region. For the infrared behavior of the interaction, we employ an Ansatz^{4,5} that is sufficiently strong to produce a realistic value for the chiral condensate of about $(240 \text{ GeV})^3$. The model parameters⁵, along with the quark masses, are fitted to give a good description of the chiral condensate, $m_{\pi/K}$ and f_{π} . The obtained results for the light vector meson masses are within 5% of their experimental values, and the vector meson electroweak decay constants are within 9% of the data⁵.

This truncation preserves both the vector Ward-Takahashi identity [WTI] for the $q\bar{q}\gamma$ vertex and the axial-vector WTI, independent of the details of the effective interaction. The latter ensures the existence of massless pseudoscalar mesons associated with dynamical chiral symmetry breaking^{4,6}. In combination with impulse approximation, the former ensures electromagnetic current conservation³.

2. Meson Form Factors

In impulse approximation, meson form factors are generically described by

$$I^{abc}(P, Q, K) = N_c \int \frac{d^4 q}{(2\pi)^4} \text{Tr} [S^a(q) \Gamma^{a\bar{b}}(q, q'; P) S^b(q') \Gamma^{b\bar{c}}(q', q''; Q) S^c(q'') \Gamma^{c\bar{a}}(q'', q; K)], \quad (5)$$

where $q - q' = P$, $q' - q'' = Q$, $q'' - q = K$, and momentum conservation dictates $P + Q + K = 0$. In Eq. (5), S^i is the dressed quark propagator with flavor index i , and $\Gamma^{i\bar{j}}(k, k'; P)$ stands for a generic vertex function with incoming quark flavor j and momentum k' , and outgoing quark flavor i and momentum k . Depending on the specific process under consideration, this vertex function could be a meson BSA or a quark-photon vertex. In the calculations discussed below, the propagators and the vertices are all obtained as solutions of their respective DSE in rainbow-ladder truncation, without adjusting any of the model parameters.

2.1. Pion and kaon elastic form factors

There are two diagrams that contribute to meson electromagnetic form factors: one with the photon coupled to the quark and one with the photon coupled to the antiquark respectively. With photon momentum Q , and incoming and outgoing meson momenta $P \mp Q/2$, we can define a form factor for each of these diagrams³

$$2 P_\nu F_{a\bar{b}\bar{b}}(Q^2) = I_\nu^{abb}(P - Q/2, Q, -(P + Q/2)). \quad (6)$$

We work in the isospin symmetry limit, and thus $F_\pi(Q^2) = F_{u\bar{u}u}(Q^2)$. The K^+ and K^0 form factors are given by $F_{K^+} = \frac{2}{3}F_{u\bar{s}u} + \frac{1}{3}F_{u\bar{s}\bar{s}}$ and $F_{K^0} = -\frac{1}{3}F_{d\bar{s}d} + \frac{1}{3}F_{d\bar{s}\bar{s}}$ respectively.

Our result for $Q^2 F_\pi$ and F_{K^+} are shown in Fig. 1, together with the experimental data^{7,8,9,10}. Up to about $Q^2 = 2 \text{ GeV}^2$, our result for F_π can be described very well by a monopole with our calculated ρ -mass, $m_\rho = 742 \text{ MeV}$ (note that our calculated ρ -mass is slightly below the experimental

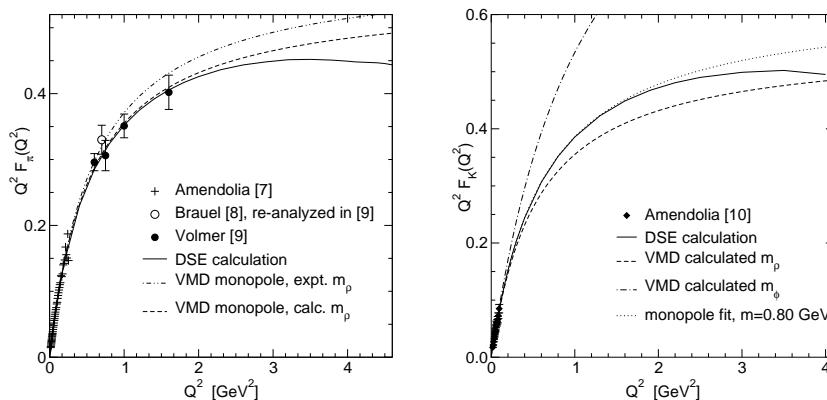


Figure 1. On the left, our result for $Q^2 F_\pi(Q^2)$, and right, our curve for $Q^2 F_{K^+}(Q^2)$.

value). Above this value, our curve starts to deviate more and more from this naive VMD monopole. Our result is in excellent agreement with the most recent JLab data⁹; it would be very interesting to compare with future JLab data in the 3 to 5 GeV² range, where we expect to see a significant deviation from the naive monopole behavior.

Also our results for F_K agree with the available experimental data¹⁰, as do both the neutral and the charged kaon charge radius³. Again, our curve for F_K can be fitted quite well by a monopole up to about $Q^2 = 2 \text{ GeV}^2$, see Fig. 1; above 2 GeV², we see a clear deviation from a monopole behavior. Also for this form factor it would be interesting to compare with future JLab data at larger Q^2 .

2.2. Vector-pseudoscalar-photon transitions

We can describe the radiative decay of the vector mesons using the same loop integral, Eq. (5), this time with one vector meson BSA, one pseudoscalar BSA, and one $q\bar{q}\gamma$ -vertex¹¹. The on-shell value gives us the coupling constant. For virtual photons, we can define a transition form factor $F_{VP\gamma}(Q^2)$, normalized to 1 at $Q^2 = 0$, which can be used in estimating meson-exchange contributions to hadronic processes^{12,13}.

In the isospin limit, both the $\rho^0 \pi^0 \gamma$ and $\rho^\pm \pi^\pm \gamma$ vertices are given by

$$\frac{1}{3} I_{\mu\nu}^{uuu}(P, Q, -(P+Q)) = \frac{g_{\rho\pi\gamma}}{m_\rho} \epsilon_{\mu\nu\alpha\beta} P_\alpha Q_\beta F_{\rho\pi\gamma}(Q^2), \quad (7)$$

where P is the ρ momentum. The $\omega \pi \gamma$ vertex is a factor of 3 larger, due to the difference in isospin factors. For the $K^* \rightarrow K\gamma$ decay, we have to add two terms: one with the photon coupled to the \bar{s} -quark and one with the photon coupled to the u - or d -quark, corresponding to the charged or neutral K^* decay respectively¹¹.

As Eq. (7) shows, it is $g_{VP\gamma}/m_V$ that is the natural outcome of our calculations; therefore, it is this combination that we give in Table 1, together with the corresponding partial decay widths¹¹. The agreement between theory and experiment for $g_{VP\gamma}/m_V$ is within about 10%, except for the discrepancy in the charged $K^* \rightarrow K\gamma$ decay for which we have no explanation. Likewise the large difference between the neutral and charged ρ decay width is beyond the reach of the isospin symmetric impulse approximation.

Table 1. Vector meson radiative decays: g/m in GeV⁻¹ and $\Gamma_{V \rightarrow P\gamma}$ in keV.

	g/m	$\Gamma_{\rho^\pm \pi^\pm \gamma}$	g/m	$\Gamma_{\omega \pi \gamma}$	g/m	$\Gamma_{K^{*\pm} K^\pm \gamma}$	g/m	$\Gamma_{K^{*0} K^0 \gamma}$
calc.	0.69	53	2.07	479	0.99	90	1.19	130
expt. ¹⁴	0.74	68	2.31	717	0.83	50.3	1.28	116

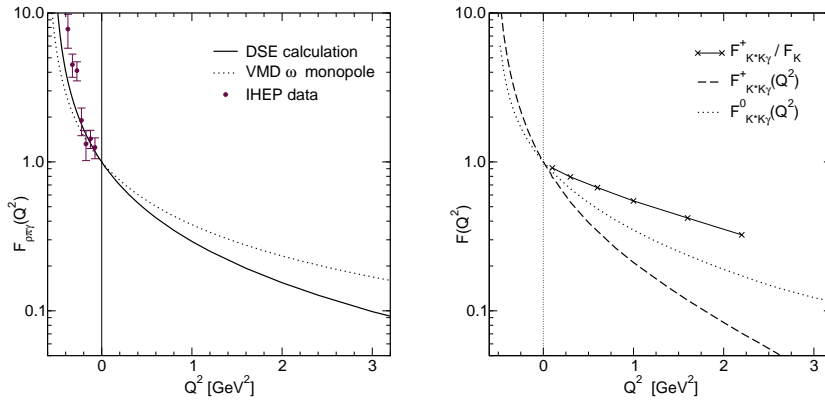


Figure 2. On the left, our result for $F_{\omega\pi\gamma}(Q^2)$ with experimental data¹⁵, and right, our curve for the charged and neutral $F_{K^*K\gamma}(Q^2)$.

Note that part of the difference between the experimental and calculated decay width comes from the phase space factor because our calculated vector meson masses deviate up to 5% from the physical masses.

The corresponding transition form factors are shown in Fig. 2. In contrast to the elastic form factors, these transition form factors fall off significantly faster than a VMD-like monopole; our numerical results¹¹ for $F_{\rho\pi\gamma}(Q^2)$ suggest an asymptotic behavior of $1/Q^4$. Only in the timelike region, near the vector meson pole, do we see a clear VMD-like behavior.

For the $K^*K\gamma$ form factor the situation is more complicated due to the interference of the diagrams with the photon coupled to the s -quark and to the u - or d -quark. This causes the charged form factor to fall off much more rapidly than both the neutral $K^*K\gamma$ form factor and the elastic form factor $F_K(Q^2)$, as can be seen from Fig. 2. The latter implies that the contribution to charged kaon electroproduction from intermediate K^* exchange gets suppressed with increasing Q^2 compared to the contribution from virtual kaon exchange.

2.3. Remarks on meson electroproduction

We can use this approach to estimate the range of validity of meson-dominance models¹¹. For off-shell pions, the meson-dominance assumption appears to be quite good for spacelike momentum transfer of the order of $t \sim 0.1 \text{ GeV}^2$. On the other hand, for heavier mesons such as kaons or ρ -mesons, the naive meson-dominance assumption introduces significant errors, even at small spacelike values of $t \sim 0.2 \text{ GeV}^2$. In addition, any

meson-exchange model to describe meson electroproduction necessarily introduces off-shell ambiguities. Clearly, a microscopic description is needed.

Any microscopic description of meson-electroproduction requires a quark-gluon description of the nucleon. It is a difficult task to combine such a description with the meson form factors considered here. Recently, significant progress in describing processes involving four external particles has been made, using the rainbow-ladder truncation of the DSEs, in conjunction with an extension of the impulse approximation¹⁶. This approach incorporates the non-analytic effects of intermediate meson-exchange contributions while avoiding ambiguous off-shell definitions. It has successfully been applied to π - π scattering, where we can identify the non-analytic contributions from σ - and ρ -exchange to the S-wave and P-wave scattering amplitudes respectively¹⁷. Furthermore, it was shown to reproduce the correct chiral limit¹⁶. We plan to extend this approach to describe processes such as $\gamma\pi\pi\pi$, pion compton scattering, and meson electroproduction.

Acknowledgments

Most of this work was done in collaboration with Peter Tandy. This work was funded by the US Department of Energy under grants No. DE-FG02-96ER40947 and DE-FG02-97ER41048, and benefitted from the resources of the National Energy Research Scientific Computing Center.

References

1. C. D. Roberts and S. M. Schmidt, Prog. Part. Nucl. Phys. **45S1**, 1 (2000); R. Alkofer and L. von Smekal, Phys. Rept. **353**, 281 (2001);
2. P. Maris and P. C. Tandy, Phys. Rev. C **61**, 045202 (2000).
3. P. Maris and P. C. Tandy, Phys. Rev. C **62**, 055204 (2000).
4. P. Maris and C. D. Roberts, Phys. Rev. C **56**, 3369 (1997).
5. P. Maris and P. C. Tandy, Phys. Rev. C **60**, 055214 (1999).
6. P. Maris, C. D. Roberts and P. C. Tandy, Phys. Lett. B **420**, 267 (1998).
7. S. R. Amendolia *et al.*, Nucl. Phys. B **277**, 168 (1986).
8. P. Brauel *et al.*, Z. Phys. **C3**, 101 (1979).
9. J. Volmer *et al.*, Phys. Rev. Lett. **86**, 1713 (2001).
10. S. R. Amendolia *et al.*, Phys. Lett. B **178**, 435 (1986).
11. P. Maris and P. C. Tandy, Phys. Rev. C **65**, 045211 (2002).
12. P. C. Tandy, Prog. Part. Nucl. Phys. **39**, 117 (1997).
13. J. W. Van Orden, N. Devine and F. Gross, Phys. Rev. Lett. **75**, 4369 (1995).
14. Particle Data Group, C. Caso *et al.*, Eur. Phys. J. **C3**, 1 (1998).
15. R. I. Dzhelyadin *et al.*, Phys. Lett. B **102**, 296 (1981) [JETP Lett. **33**, 228 (1981)].
16. P. Bicudo *et al.*, Phys. Rev. D **65**, 076008 (2002).
17. S. Cotanch and P. Maris, in preparation.